https://doi.org/10.5194/egusphere-2026-4525
Preprint. Discussion started: 22 September 2026

An argument for using a variable Schmidt number exponent based on direct measurements of air–sea gas exchange

Simon F. Hauser[1], Yuanxu Dong[3], Anneke ten Doeschate[4], Kevin McGraw[2], Brian Ward[2], and Leonie Esters[1]

[1]Institute of Geosciences, Meteorology Section, University of Bonn, Germany
[2]AirSea Laboratory, School of Natural Sciences, University of Galway, Ireland
[3]Laboratoire de Météorologie Dynamique, LMD-IPSL, École Normale Supérieure, Université PSL, École polytechnique, Institut Polytechnique de Paris, Sorbonne Université, CNRS, Paris, France
[4]Rockland Scientific, Victoria, BC, Canada

Abstract.

Air–sea gas exchange is typically parametrized as a function of wind speed using the gas transfer velocity k, which is normalized to a specific Schmidt number (Sc). The Sc describes the ratio of diffusive momentum transport to diffusive mass transport in a fluid and can be parameterized as a function of water temperature. We conducted coincident eddy covariance (EC) measurements of k and turbulent kinetic energy dissipation rate (ϵ) measurements by an upwardly rising microstructure profiler. Since $k \propto Sc^{-n}$ with the Sc exponent n and $k \propto \epsilon^{1/4}$, we can derive n based on these measurements. Here, we obtain a linear parameterization of n as a function of wind speed: $n(U_{10}) = -0.0136\,U_{10} + 2/3$. Allowing n to vary instead of using the commonly assumed value $n = 1/2$ can have a significant impact on global k. To quantify this effect, $n(U_{10})$ was combined with the ERA5 reanalysis product and k was normalized to $Sc = 660$. Global k_{660} is estimated to decrease by about 12 % when k_{660} is determined using the dual tracer method, but to increase by 5 % or less for EC-derived estimates. To assess the resulting effect on air–sea CO_2 fluxes, $n(U_{10})$ was subsequently applied to an average of global fCO_2-based flux data products for 2023. Based on an EC-derived k_{660} parameterization, we find substantial relative increases in flux in large areas of the tropical and subtropical oceans, while global net uptake increases by only about 1 %. Due to the direct dependence of k on n, using $n(U_{10})$ in the dual tracer method results in a significant relative decrease in flux across large parts of the global ocean, while global net uptake decreases by about 5 %. We suggest applying a variable n under low-wind conditions, particularly for the EC method at low water temperatures or the dual tracer method at high water temperatures.

1 Introduction

The ocean absorbs 25–30% of anthropogenic carbon emissions (Friedlingstein et al., 2025) and therefore plays an outsize role in climate regulation. Estimates of the global ocean–atmosphere CO_2 flux rely on parameterizations of the gas transfer velocity k, which links the air–sea difference in CO_2 concentration to the flux. It characterizes the efficiency of the gas transfer across the air–sea interface and is primarily controlled by turbulent processes in the waterside boundary layer. However, k is typically parametrized as a function of wind speed because global wind speed products are readily available (Hersbach et al.,

https://doi.org/10.5194/egusphere-2026-4525
Preprint. Discussion started: 22 September 2026

2023; Mears et al., 2022). These wind speed based parameterizations have been derived from natural ^{14}C disequilibrium and bomb ^{14}C inventories (Wanninkhof, 1992, 2014), the $^{3}He/SF_6$ dual tracer (DT) method (Nightingale et al., 2000; Ho et al., 2006) and eddy covariance (EC) measurements (e.g. Yang et al., 2022; Dong et al., 2024). For the DT method to estimate k, Helium 3 (^{3}He) and sulfur hexafluoride (SF_6) are used as volatile deliberate tracers, and k is determined from the temporal evolution of the ratio of the tracer concentrations in the water (Watson et al., 1991; Wanninkhof et al., 2009; Ho et al., 2011). The DT method has been used to determine k in a seagrass ecosystem (Dobashi and Ho, 2023), coastal waters (Wanninkhof et al., 1993; Nightingale et al., 2000), and the open ocean (Wanninkhof et al., 2004; Ho et al., 2006, 2011; Ho and Wanninkhof, 2016). With the EC method, air–sea gas fluxes can be obtained directly from the covariance of vertical wind velocity and gas mixing ratio. These flux measurements and coincident measurements of the air–sea difference in partial gas pressure can then be used to derive k. In recent years, the EC method has been used to study air–sea gas exchange over lakes (Mammarella et al., 2015; Erkkilä et al., 2018; Esters et al., 2021; Golub et al., 2023), coastal waters (Yang et al., 2016; Gutiérrez-Loza et al., 2022; Dong et al., 2026), and the open ocean (Landwehr, 2015; Landwehr et al., 2015; Butterworth and Miller, 2016; Bell et al., 2017; Blomquist et al., 2017; Brumer et al., 2017; Landwehr et al., 2018; Dong et al., 2021b; Yang et al., 2022; Dong et al., 2024). Uncertainties in the parameterization of k are the main source of uncertainty in data-product estimates of air–sea CO_2 fluxes for most ocean regions (Ford et al., 2024; Gloege and Eisaman, 2025). While the commonly used wind speed based parameterizations of k have a quadratic dependence (e.g., Wanninkhof, 1992, 2014), some also incorporate an additional constant or linear term (e.g., Nightingale et al., 2000; Yang et al., 2022; Dong et al., 2024). Gloege and Eisaman (2025) assumed a quadratic term only and assigned an uncertainty of 20 % on the scaling factor. The relative standard uncertainty on k parameterizations based on EC measurements of the air–sea CO_2 flux is about 7 % at moderate wind speeds (Yang et al., 2022). Woolf et al. (2019) estimated the standard uncertainty in the DT-based k parameterizations to be 5–10 %.

To enable consistent comparisons across gases and temperature regimes, wind speed based parameterizations of k are typically normalized to a specific Schmidt number, $Sc = \nu/D$, where ν denotes the kinematic viscosity of water and D the molecular diffusion coefficient of the gas. The Schmidt number describes the ratio of diffusive momentum transport to diffusive mass transport in a fluid and can be parameterized as a function of temperature for seawater and freshwater (Wanninkhof, 2014). The most common choices for normalization are $Sc = 600$ (e.g., Nightingale et al., 2000; Ho et al., 2006) and $Sc = 660$ (e.g., Wanninkhof, 2014; Yang et al., 2022), which approximately correspond to the Schmidt numbers of CO_2 at 20 °C for freshwater and seawater, respectively. Therefore, $Sc = 660$ is used hereafter. To normalize k, it is multiplied by a factor $(660/Sc)^{-n}$, where n is the Sc exponent. By integrating Ficks's first law of diffusion, while also accounting for vertical turbulent transport (see Sect. 2 for details), $n = 1/2$ is obtained for a wavy water surface and $n = 2/3$ for a smooth water surface (Jähne and Haußecker, 1998; Jähne, 2009).

The resulting differences in k can be substantial. For example, using $k \propto \mathrm{Sc}^{-1/2}$ instead of $k \propto \mathrm{Sc}^{-2/3}$ for $Sc = 600$ can increase k by about a factor of 3 (Jähne, 2009). In laboratory experiments, the transition was found to be smooth when studying n as a function of wind speed or friction velocity (Richter and Jähne, 2011; Krall, 2013), and as a function of a surface stress ratio and a scaling constant (McKenna and McGillis, 2004). In field experiments, it is difficult to measure n, so a constant n is chosen. For open-ocean and coastal waters, $n = 1/2$ is typically applied, as a wavy surface is assumed. Investigations on

https://doi.org/10.5194/egusphere-2026-4525
Preprint. Discussion started: 22 September 2026

the relationship between k and turbulence in lakes (Gålfalk et al., 2013; Wang et al., 2015; Zhao et al., 2018), in laboratory experiments (Li et al., 2025), and based on numerical simulations (Di Giorgio et al., 2025), also assumed a constant $n = 1/2$. An exception to this is Esters et al. (2017), where a variable n was implemented based on measured k for dimethyl sulfide (DMS) and near-surface turbulence data in the North Atlantic and the Pacific Ocean. Another exception is Nagel et al. (2019), who used a variable n based on laboratory experiments to scale heat transfer velocities measured in the Baltic Sea to gas transfer velocities.

Based on Guérin et al. (2007) and Bade (2009), several recent studies on the air–sea gas exchange of CO_2 in reservoirs and fluvial networks have used a step function with $n = 2/3$ for $U_{10} < U_{step}$ and $n = 1/2$ for $U_{10} > U_{step}$ with a transition wind speed U_{step} of $3.7\,\mathrm{m\,s^{-1}}$ (Paranaíba et al., 2018; Bodmer et al., 2025) or $3\,\mathrm{m\,s^{-1}}$ (Obertegger et al., 2024). In the original source that Guérin et al. (2007) and Bade (2009) refer to, Liss and Merlivat (1986) suggested using $n = 2/3$ for a smooth surface regime defined by $U_{10} < 3.6\,\mathrm{m\,s^{-1}}$ and $n = 1/2$ for a rough surface regime defined by $U_{10} > 3.6\,\mathrm{m\,s^{-1}}$. In support of this, laboratory results from Jähne et al. (1987) also suggested a relatively sudden change of regimes at a waterside friction velocity of around $u_{*w} = 0.004\,\mathrm{m\,s^{-1}}$. However, the results of more recent laboratory experiments (Richter and Jähne, 2011; Krall, 2013) and field studies (Esters et al., 2017) indicate that the transition from $n = 2/3$ to $n = 1/2$ is rather smooth and does not behave like a step function.

In this study, we use the dependence of k on n (Sect. 2) to estimate a variable n from near-surface measurements of the turbulent kinetic energy dissipation rate (ϵ) and EC-derived k (Sect. 3). The resulting n is expressed as a function of wind speed (Sect. 4.1). We then apply $n(U_{10})$ to investigate the impact of a variable n on k obtained from the EC and DT methods under various oceanic conditions (Sect. 4.2). To do so, we use adaptation factors that describe the ratio of k using a variable n and k using $n = 1/2$. Additionally, we examine the effect of a variable n on ocean-atmosphere CO_2 fluxes (Sect. 4.3). In Sect. 2, we first provide background on how k depends on the Sc exponent and then present four methods of determining k.

2 Theoretical background

Assuming stationarity, homogeneity, and the absence of chemical sources and sinks, we obtain the inverse of the gas transfer velocity k by integrating Fick's first law of diffusion while accounting for vertical turbulent transport (Jähne, 2009; Richter and Jähne, 2011):

$$\frac{1}{k} = \int_0^{Z_r} \frac{1}{D + K_c(z)}\,\mathrm{d}z, \tag{1}$$

with the molecular diffusion coefficient D and the turbulent diffusion coefficient $K_c(z)$. The integration is performed from the surface to a reference depth Z_r representing the bulk. For a smooth water surface, the Reichardt approach with $K_c(z) = a\frac{u_{*w}^3}{\nu^2}z^3$ close to the surface can be applied, which is analogous to the transfer of mass to a smooth solid wall (Reichardt, 1951; Deacon, 1977; Jähne, 1980; Coantic, 1986). Here, a is a dimensionless constant and u_{*w} is the waterside friction velocity. This approach is especially valid if a film cover is present at the water surface that inhibits velocity fluctuations. Inserting $K_c(z)$ into Equation

https://doi.org/10.5194/egusphere-2026-4525
Preprint. Discussion started: 22 September 2026

1, substituting $x = (a\,\frac{u_{*w}^3}{\nu^3} Sc)^{1/3} z$, and extending the upper integration limit, exploiting the fact that the contributions beyond Z_r are negligible, leads to:

$$\frac{1}{k} = \frac{Sc^{2/3}}{(a\,u_{*w}^3)^{1/3}} \int_0^\infty \frac{1}{1+x^3}\,\mathrm{d}x. \tag{2}$$

The integral can be evaluated using partial fraction decomposition, yielding:

$$k = \frac{3\sqrt{3}}{2\pi} a^{1/3}\, u_{*w}\, Sc^{-2/3}. \tag{3}$$

For a free, wavy water surface, velocity fluctuations at the surface are possible and the turbulent diffusion coefficient can be described as $K_c(z) = a\frac{u_{*w}^2}{\nu} z^2$ (Jähne and Haußecker, 1998; Jähne, 2009). These fluctuations occur through the generation of wind waves and lead to the dilation or contraction of surface elements (Jähne, 2009). Compared to the case of a smooth water surface, where $K_c(z) \propto z^3$, we now have $K_c(z) \propto z^2$ and the dependencies on u_{*w} and ν have been adjusted accordingly to ensure dimensional consistency. Inserting $K_c(z)$ into Equation 1 and substituting $x = (a\,\frac{u_{*w}^2}{\nu^2} Sc)^{1/2} z$ results in

$$\frac{1}{k} = \frac{Sc^{1/2}}{(a\,u_{*w}^2)^{1/2}} \int_0^\infty \frac{1}{1+x^2}\,\mathrm{d}x, \tag{4}$$

which leads to:

$$k = \frac{2}{\pi} a^{1/2}\, u_{*w}\, Sc^{-1/2}. \tag{5}$$

Therefore, we obtain:

$$k \propto \begin{cases} \mathrm{Sc}^{-2/3}, & \text{for a smooth surface,} \\ \mathrm{Sc}^{-1/2}, & \text{for a wavy surface.} \end{cases} \tag{6}$$

As both of the above cases correspond to boundary values of the exponent, they should be considered limiting cases.

The air–sea gas flux F is related to k and the fugacity difference of the gas in the water and in the air $(f^{\text{water}} - f^{\text{air}})$ in units of atm:

$$F = k_{660} K_0 \left(f^{\text{water}} - f^{\text{air}}\right) \left(\frac{Sc}{660}\right)^{-n}. \tag{7}$$

Here, k_{660} is normalized to $Sc = 660$, and the solubility of the gas in saltwater $K_0 = K_0(T, S)$ in $\mathrm{mol\,m^{-3}\,atm^{-1}}$ is a function of temperature and salinity with given coefficients (Wanninkhof, 2014). For poorly soluble gases, k_{660} is related to k at ambient Schmidt number via

$$k_{660} = k \left(\frac{660}{Sc}\right)^{-n}. \tag{8}$$

https://doi.org/10.5194/egusphere-2026-4525
Preprint. Discussion started: 22 September 2026

2.1 Eddy covariance method

With the EC method, F can be obtained from the covariance $\overline{w'c'}$ of the vertical wind velocity w and the gas mixing ratio c in ppm:

$$F = \rho_a \overline{w'c'}. \tag{9}$$

Here, ρ_a denotes the dry-air density in $\mathrm{mol\,m^{-3}}$, and w' and c' are the fluctuating components of w and c. According to Equation 7, k_{EC} can then be derived from the flux:

$$k_{EC} = \frac{F}{K_0\,(f^{\text{water}} - f^{\text{air}})}. \tag{10}$$

Note that k_{EC} is given at ambient Sc, unless it is normalized to $Sc = 660$ via Equation 8.

2.2 Dual tracer method

Alternatively, in the DT method, k is determined from the temporal evolution of the ratio of the tracer concentrations $c(^3He)$ and $c(SF_6)$, with scaling based on the Sc ratio of of the two gases (Watson et al., 1991; Nightingale et al., 2000; Wanninkhof et al., 2009; Ho et al., 2011):

$$k_{DT} = -h\frac{d}{dt}\left(\ln\left(\frac{c(^3He)}{c(SF_6)}\right)\left[1 - \left(\frac{Sc(SF_6)}{Sc(^3He)}\right)^{-n}\right]^{-1}\right). \tag{11}$$

Here, t denotes the time and h is the mixed layer depth. To make the results comparable with other measurements, k_{DT} has to be normalized to $Sc = 660$ following Equation 8. An important conceptual difference compared to the EC method is that k_{DT} explicitly depends on n, whereas in the EC approach, a dependence only occurs in the Sc normalization factor. The sensitivity to n is further increased by the large difference between $Sc(^3He)$ and $Sc(SF_6)$. At 20 °C, $Sc(^3He)$ is approximately 150, whereas $Sc(SF_6)$ is approximately 1000.

2.3 ^{14}C method

By monitoring the ^{14}C levels in the atmosphere and in the ocean, k can be determined utilizing the ^{14}C released into the atmosphere during bomb testing. These estimates have been refined over time, through advances in the separation of natural ^{14}C from bomb-^{14}C, improved spatial resolution, the application of global ocean circulation models, and the inclusion of $^{14}CO_2$ fluxes from the ocean to the atmosphere (Wanninkhof, 1992; Sweeney et al., 2007; Naegler, 2009; Wanninkhof, 2014). Based on these estimates, parameterizations of the form

$$k_{^{14}C} = \gamma\left(\frac{Sc(CO_2)}{660}\right)^{-n}\langle U_{10}^2\rangle \tag{12}$$

are derived, with the mean quadratic wind speed $\langle U_{10}^2\rangle$ and a dimensionless factor γ (Sweeney et al., 2007):

$$\gamma = \frac{\Delta\mathrm{Inv}\left(\text{Bomb DI}^{14}\mathrm{C}\right)}{\int\int\int\left(\frac{Sc(CO_2)}{660}\right)^{-n} U_{10}^2\,K_0\,\Delta p^{14}CO_{2\text{bomb}}\,dx\,dy\,dt}. \tag{13}$$

https://doi.org/10.5194/egusphere-2026-4525
Preprint. Discussion started: 22 September 2026

All quantities in the integral in the denominator depend on the time t and the spatial coordinates x and y, including the partial pressure difference of the bomb-produced $^{14}CO_2$ in the water and in the air, $\Delta p^{14}CO_{2\mathrm{bomb}}$. The change of ocean bomb radiocarbon inventory in the considered time period is denoted by $\Delta\mathrm{Inv}\left(\mathrm{Bomb\ DI}^{14}\mathrm{C}\right)$.

2.4 Small-eddy model

Lamont and Scott (1970) used the surface renewal theory, which assumes that turbulent eddies periodically transport water from deeper layers to the surface, to derive a direct relationship between k and the turbulent kinetic energy (TKE) dissipation rate ϵ $[\mathrm{m}^2/\mathrm{s}^3]$ in the water:

$$k_{SEM} = A(\epsilon\nu)^{1/4} Sc^{-n}. \tag{14}$$

This relation is also known as the small-eddy model (SEM) and has been used in recent studies relating k and ϵ (Wang et al., 2015; Esters et al., 2017; Zhao et al., 2018; Li et al., 2025). The dimensionless proportionality factor A is set to $A = 0.4$ for ϵ measured directly at the water surface (Lamont and Scott, 1970). Katul and Liu (2017) showed that Equation (14) can also be derived from dimensional analysis or a vertical velocity structure function approach, which underlines the robustness of this scaling.

3 Observations

The data used for this analysis was collected during two oceanographic campaigns: Knorr11 in the North Atlantic and BELAS in the Labrador Sea. The Knorr11 field campaign was conducted from late June to mid-July 2011. Air–sea gas fluxes and concentration differences were measured for dimethyl sulfide (DMS) and CO_2. Details of the measurement setup and the data analysis technique can be found in Miller et al. (2010), Landwehr (2015), Landwehr et al. (2015), Bell (2015), and the appendix of Bell et al. (2017). We used EC data from Bell et al. (2017) of the transfer velocity of DMS at hourly intervals and combined it with coincident Air–Sea Interaction Profiler (ASIP) data of ϵ. Both are displayed in Fig. 1. ASIP is an autonomous upwardly rising vertical profiler, which was built to carry out microstructure measurements of the ocean surface boundary layer (Ward et al., 2014). ASIP is equipped with a set of sensors including temperature, conductivity, and shear. The magnitude of ϵ can be estimated from the microstructure shear measurements following the analysis methods described in Lueck et al. (2024). For ϵ close to the surface, the uppermost ϵ bin is used, with a resolution of about 0.5 m (Ward et al., 2014). During the Knorr11 campaign, ASIP was deployed on four occasions and the dataset consists of 115 profiles in total. To make the EC data comparable to ϵ measured with ASIP, k and U_{10} were linearly interpolated to the times when ASIP reached the surface, using the two nearest data points in time for each profile. The analysis only uses DMS gas transfer velocity data from the Knorr11 campaign, not CO_2 data. This is because only 14 hours with coincident k_{CO_2} and ASIP ϵ measurements are available over a total of four days to determine the variable Sc exponent. Sea surface temperature and salinity for Knorr11 were taken from Bell et al. (2017) and used to derive the kinematic viscosity ν and the Sc for both $^3\mathrm{He}$ and SF_6 based on the parameterizations by Wanninkhof (2014).

https://doi.org/10.5194/egusphere-2026-4525
Preprint. Discussion started: 22 September 2026

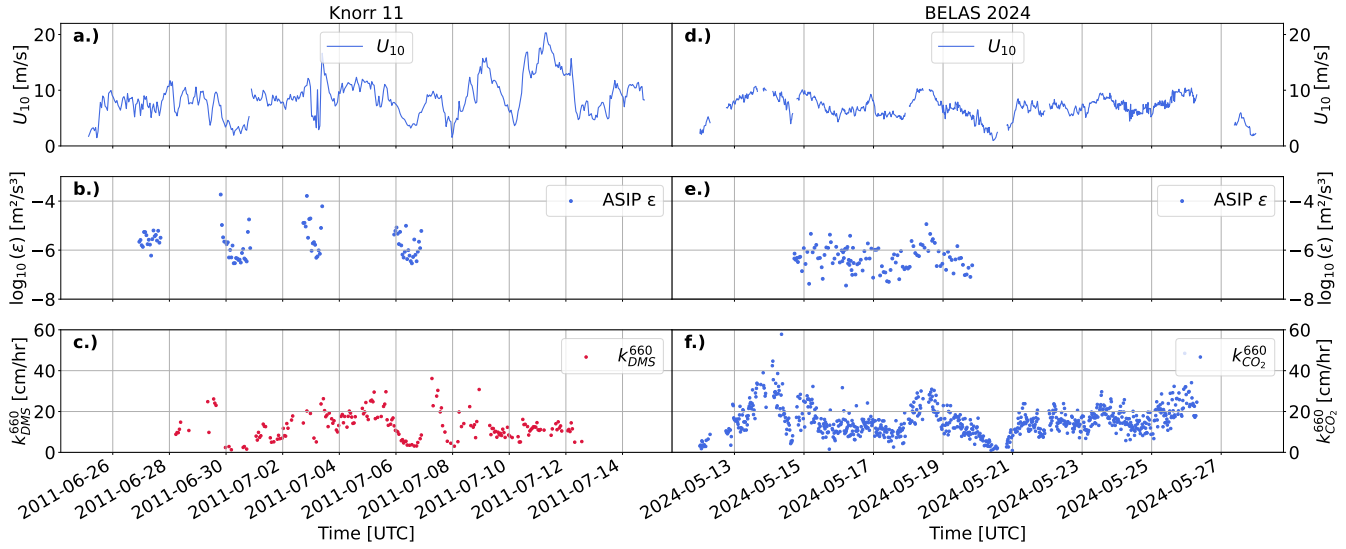

Figure 1. Time series for Knorr11 (a.-c.) and BELAS (d.-f.): a.) In situ U_{10}, b.) ASIP ϵ close to the surface, c.) DMS gas transfer velocity k_{DMS} normalized to $Sc = 660$ using a constant Sc exponent $n = 1/2$, d.) in situ U_{10}, e.) ASIP ϵ close to the surface, and f.) $k_{\mathrm{CO_2}}$ normalized to $Sc = 660$ using a constant Sc exponent $n = 1/2$. Note the different temporal resolutions of k for Knorr11 (1 h) and BELAS (20 min).

For the gas exchange of $\mathrm{CO_2}$, data from the BELAS field campaign aboard the RV *Celtic Explorer* in May 2024 was used. It was conducted to investigate the biological carbon pump in the Labrador Sea. ASIP was deployed once, collecting a total of 114 profiles. Coincident EC measurements of the air–sea $\mathrm{CO_2}$ flux $F_{\mathrm{CO_2}}$ were performed, and the partial pressure $p\mathrm{CO_2}$ in water and air was measured by an equilibrator system. From $p\mathrm{CO_2}^{\mathrm{water}}$ and $p\mathrm{CO_2}^{\mathrm{air}}$, the fugacities $f\mathrm{CO_2}^{\mathrm{water}}$ and $f\mathrm{CO_2}^{\mathrm{air}}$ were derived. Only data points with $|\Delta f\mathrm{CO_2}| = |f\mathrm{CO_2}^{\mathrm{water}} - f\mathrm{CO_2}^{\mathrm{air}}| > 40\,\mu$atm were considered for the analysis (Landwehr, 2015). The resulting $k^{660}_{\mathrm{CO_2}}$ for BELAS is shown in Fig. 1f, it was derived via Equation 7 with a constant Sc exponent of $n = 1/2$. The same linear interpolation technique used for Knorr11 was employed to estimate k and U_{10} at times where ASIP reached the surface. The solubility K_0 was calculated following the parameterization given by Wanninkhof (2014), while ν and Sc were derived from the ASIP water temperature and salinity closest to the surface.

4 Results and discussion

4.1 Fitting a variable Schmidt number exponent

As mentioned above, n is expected to range between the boundary values of $1/2$ and $2/3$. There are no theoretical constraints on the shape of the transition, except that is is expected that $n = 2/3$ holds for $U_{10} = 0$. Here, a linear function of U_{10} is chosen to describe the continuous transition between $n = 2/3$ and $n = 1/2$, as it is the simplest approach:

$$n(U_{10}) = BU_{10} + \frac{2}{3}. \tag{15}$$

https://doi.org/10.5194/egusphere-2026-4525
Preprint. Discussion started: 22 September 2026

We are using EC-derived k and measured ϵ for the fit of $n(U_{10})$, which leads to the following fit function (see Eq. 14):

$$k = A(\epsilon\nu)^{1/4}\,(Sc)^{-(BU_{10}+2/3)}\,, \tag{16}$$

with the scaling parameter A and the slope parameter B. The resulting fit functions for n from this work are summarized in Table 1. The results from Knorr11 and BELAS (Fig. 2) agree with previous laboratory results by Krall (2013) using the the Aelotron circular wind-wave flume. Four independent measurement series were conducted for the surfactant-free case (clean), one series for the medium surfactant case ($0.052\,\mu\,\mathrm{mol\,l^{-1}}$ Triton) and two series for the high-surfactant case ($0.26\,\mu\,\mathrm{mol\,l^{-1}}$ Triton). When fitting our data with respect to U_{10}, the agreement with the laboratory results is best for the surfactant-free case (Fig. 2). However, $n(U_{10})$ is higher than the laboratory results for the surfactant-free case for wind speeds between $3.5\,\mathrm{m\,s^{-1}}$ and $12\,\mathrm{m\,s^{-1}}$, but this difference is within the uncertainty range of the fit. Esters et al. (2017) estimated n as a function of waterside friction velocity $n(u_{*w})$, also using k_{DMS} data from the Knorr11 field experiment. Based on a different analysis and fitting procedure, they obtained $n(u_{*w}) = -0.22\log_{10}(u_{*w}) + 0.13$. Similar differences in the scaling parameters for CO_2 and DMS (Table 1) have been reported previously (Esters et al., 2017). These differences could be related to the effect of bubble-mediated gas transfer, which has a greater impact on CO_2 than on DMS (Dong et al., 2025a, b).

Table 1. Fitted parameters for BELAS and Knorr11 based on U_{10}. Note that the intercept is set to $2/3$ by construction for the fits, such that $n(U_{10}) = BU_{10} + 2/3$.

Dataset	Slope B	Intercept	Scaling A
BELAS CO_2	-0.0136 ± 0.0026	$2/3$	1.69 ± 0.27
Knorr11 DMS	-0.0135 ± 0.0029	$2/3$	0.61 ± 0.12

Our results indicate that the slope parameters for $n(U_{10})$ agree within their uncertainties for DMS and CO_2. This is expected, since the behavior of n is not supposed to depend on the tracer gas used, at least for poorly soluble gases under moderate wind conditions. We recommend using the BELAS slope parameter, in particular for wind speeds in the range 4-10 $\mathrm{m\,s^{-1}}$. If $n(U_{10})$ falls below $1/2$, n should be clipped, as the exponent $1/2$ is given as a theoretical limit (Jähne and Haußecker, 1998; Jähne, 2009). By construction of the fit function, $n(U_{10})$ and cannot exceed $2/3$, as $n = 2/3$ for zero U_{10}.

4.2 Impact on gas transfer velocities

4.2.1 Eddy covariance method

To estimate the impact of using a variable n instead of a constant exponent $n = 1/2$, we define an adaptation factor α_{EC} for k originating from the EC method. It is given by the Sc normalization factor (Eq. 8) using $n(U_{10})$ divided by the normalization factor for a constant $n = 1/2$:

$$\alpha_{EC} = \frac{(660/Sc)^{-n(U_{10})}}{(660/Sc)^{-1/2}}. \tag{17}$$

https://doi.org/10.5194/egusphere-2026-4525
Preprint. Discussion started: 22 September 2026

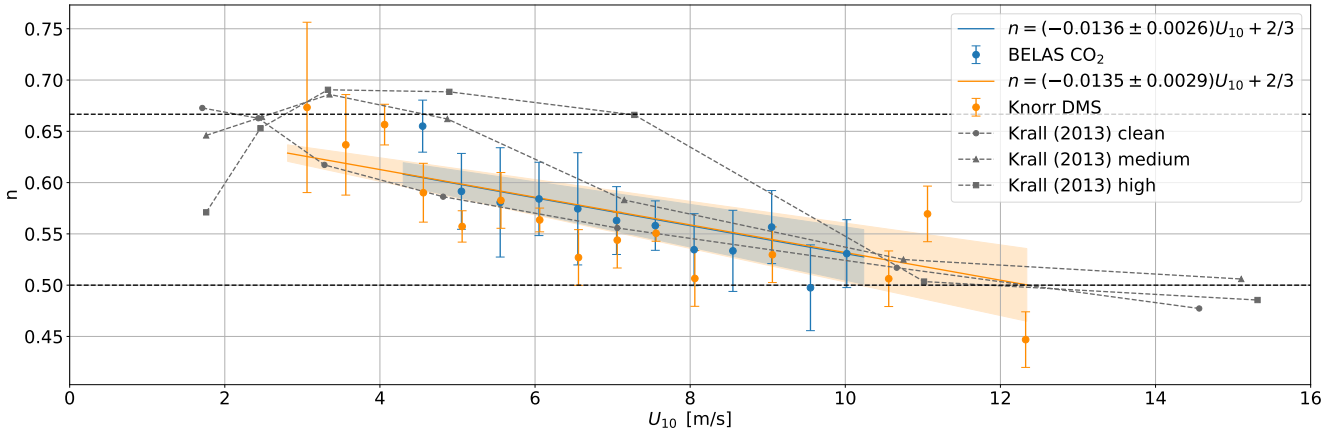

Figure 2. Fit results for the Schmidt number exponent n as a function of the 10 m wind speed U_{10}. The shadings correspond to the 1σ intervals on the fitted slopes. Binned data for n is recalculated via Equation 16 based on measured k, ϵ, and fitted scaling parameters. It is shown as error bars for CO_2 (BELAS, blue) and DMS (Knorr11, orange). For comparison, laboratory data from Krall (2013) for different surfactant conditions (clean, medium and high) is depicted. A binning with a width of $0.5\,\mathrm{m\,s^{-1}}$ with respect to U_{10} is applied. For a given bin, the corresponding uncertainty shown is either the standard deviation of the data points, or the propagated uncertainty from the uncertainty on the slope parameter, if there is only one data point in the bin.

By multiplying a given EC-derived k_{660} that was normalized to $Sc = 660$ using $n = 1/2$ with α_{EC}, we can estimate the corresponding k_{660} using a variable n for the normalization instead. An increase in k_{660} occurs when $\alpha_{EC} > 1$, while $\alpha_{EC} < 1$ indicates a decrease in k_{660}. The impact of a variable $n(U_{10})$ on k_{660} is maximal in cold water for low wind speeds (Fig. 3), where k_{660} is up to 20 % higher than when using $n = 1/2$. The general distribution of α_{EC} in (U_{10}, SST)-space is similar for applying the $n(U_{10})$ relationships from BELAS, Knorr11 and the surfactant-free laboratory measurements by Krall (2013). While both BELAS and Knorr11 were conducted in algae blooms with a potentially high surfactant concentration, this suggests that the presence of surfactants may not have had a major influence on the fit of n. With the presence of surfactants under laboratory conditions as measured by Krall (2013), the maximum shifts towards slightly higher wind speeds of 2.5–5 $\mathrm{m\,s^{-1}}$ for the medium surfactant concentration case (Fig. 3e.) and 2.5–7.5 $\mathrm{m\,s^{-1}}$ for the high surfactant concentration case (Fig. 3f.).

Implementing a step function for n with $n = 2/3$ for $U_{10} < 3.7\,\mathrm{m\,s^{-1}}$ and $n = 1/2$ for $U_{10} > 3.7\,\mathrm{m\,s^{-1}}$, as is commonly adopted in studies of reservoirs and fluvial networks (Guérin et al., 2007; Paranaíba et al., 2018; Bodmer et al., 2025), introduces a discontinuity in the normalized k of about $5 - 20$ % at the transition wind speed for water temperatures below 15 °C (Fig. 3c.). The results for BELAS and Knorr11 suggest that the transition from $n = 2/3$ to $n = 1/2$ is gradual and not adequately represented by a step function, which is in agreement with recent laboratory experiments (Krall, 2013; Nagel et al., 2019) and field studies (Esters et al., 2017). In particular, if a step function has to be applied, a reasonable choice for the transition wind speed would be 6-8 $\mathrm{m\,s^{-1}}$ instead of 3-4 $\mathrm{m\,s^{-1}}$ (see Fig. 2).

https://doi.org/10.5194/egusphere-2026-4525
Preprint. Discussion started: 22 September 2026

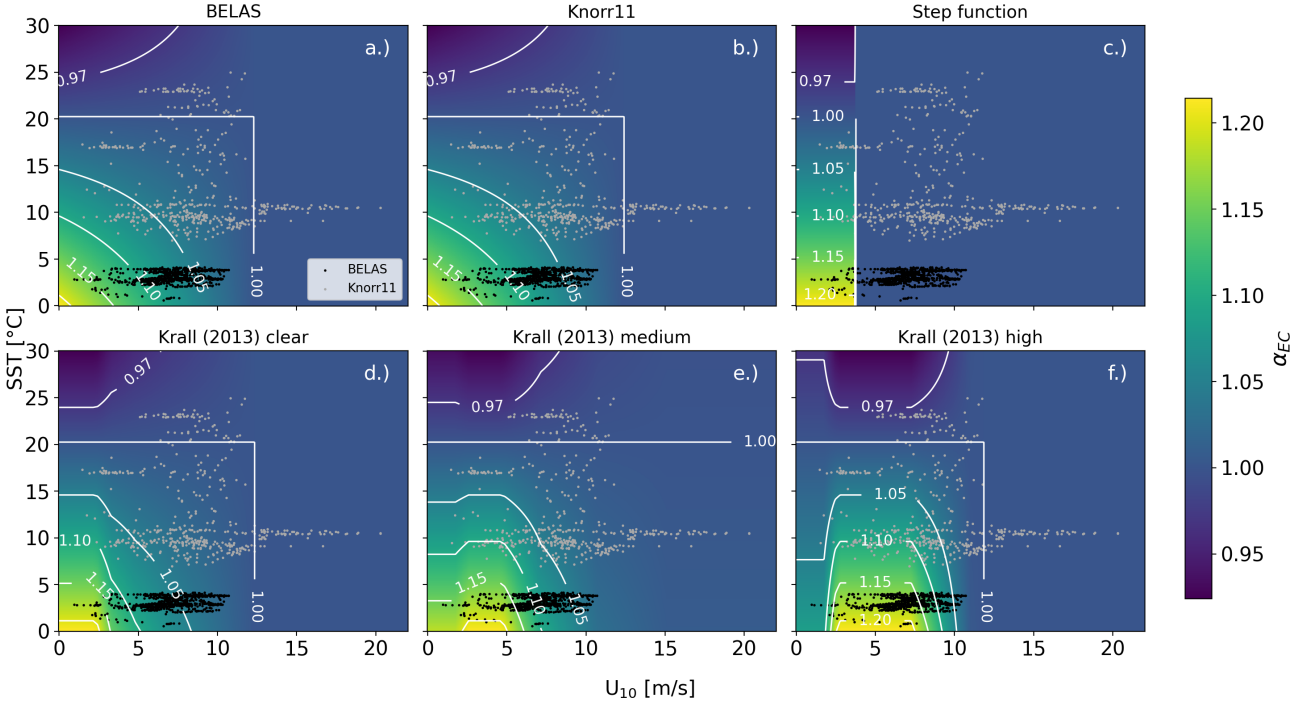

Figure 3. Relative change of EC gas transfer velocities when using a variable Schmidt number exponent compared to $n = 1/2$ for different $n(U_{10})$ relationships, based on a.) fitting BELAS CO_2 flux data, b.) fitting Knorr11 DMS gas transfer velocity data, c.) a stepfunction setting $n = 2/3$ for $U_{10} < 3.7\,\mathrm{m\,s^{-1}}$ and $n = 1/2$ for $U_{10} > 3.7\mathrm{m\,s^{-1}}$, d.) laboratory results from Krall (2013) for surfactant-free conditions, e.) medium surfactant concentrations, and f.) high surfactant concentrations at the water surface. BELAS SST and U_{10} data is shown in black and Knorr11 SST and U_{10} data is shown in grey. The relative change in k_{660} is given by the adaptation factor α_{EC} (see Equation 17).

For measurements under open-ocean conditions, a constant value of $n = 1/2$ is commonly used across all wind speeds (Butterworth and Miller, 2016; Landwehr et al., 2018; Prytherch and Yelland, 2021; Dong et al., 2021b; Yang et al., 2022; Dong et al., 2024). However, for both the BELAS and Knorr11 fits, the increase in k_{660} by applying a variable n instead of $n = 1/2$ can exceed 10 % at water temperatures below around 10 °C and wind speeds below around $6\,\mathrm{m\,s^{-1}}$ (Fig. 3a and b). Using BELAS SST and U_{10} data, there is a maximum increase of 16.3 % observed by applying α_{EC} based on the BELAS $n(U_{10})$ fit. With Knorr11 data and using the $n(U_{10})$ fit for Knorr11, the maximum increase is 8.8 % and the average impact is 2.1 %. The low average impact can be attributed to the comparatively high water temperatures, which in some instances exceed 20 ° C. For BELAS, the average impact on k is 7.1 %, as a considerable amount of the data was taken in cold waters under relatively low wind speeds (Fig. 3a). We suggest using a variable n (Table 1) for the EC method in low wind speeds and cold waters.

To assess how a variable n influences air–sea gas fluxes via k, we first normalized the BELAS k data to k_{660} via Equation 8, using $n(U_{10})$ with the BELAS slope parameter, and subsequently fitted $k_{660}(U_{10}) = a_1 U_{10}^2 + a_2$ (Fig. 4). The fit result is

https://doi.org/10.5194/egusphere-2026-4525
Preprint. Discussion started: 22 September 2026

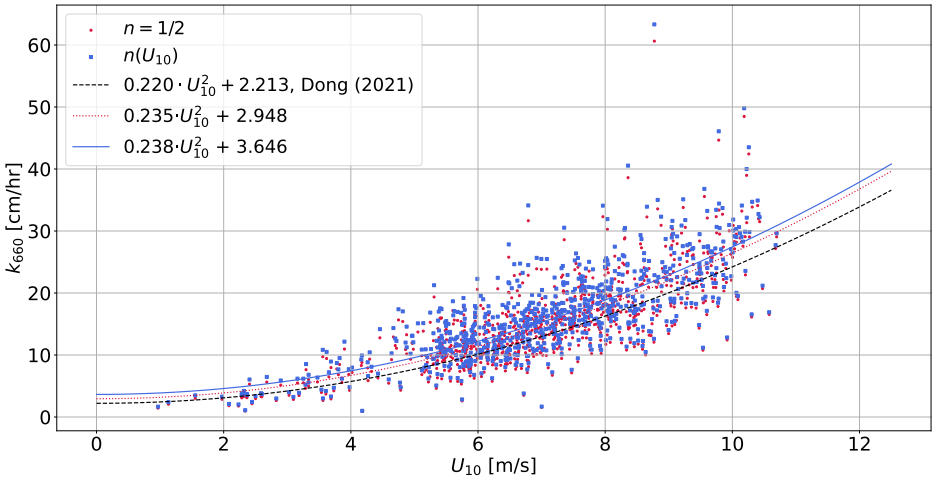

Figure 4. Fit of BELAS EC gas transfer velocity data for CO_2, normalized to $Sc = 660$ as a function of U_{10}, using $n = 1/2$ (red dots, dotted red line) and $n = n(U_{10})$ (blue squares, blue line). For the derivation of the fit functions, the data is binned in $1\,\mathrm{m\,s^{-1}}$ bins, while a single bin is used for 0-2 $\mathrm{m\,s^{-1}}$. A parameterization obtained from EC data for the Arctic (Dong et al., 2021a) is shown for comparison (dashed black line).

$k_{660}(U_{10}) = 0.238\,U_{10}^2 + 3.646$, with U_{10} given in $\mathrm{m\,s^{-1}}$ and k in $\mathrm{cm\,hr^{-1}}$. As expected from the BELAS data distribution shown in Fig. 3, where $\alpha_{EC} > 1$ for all data points, k_{660} increases for all U_{10} when a variable Sc exponent is used. The impact of using a variable n on the derivation of air–sea gas fluxes via Equation 7 is estimated in Sect. 4.3.1, based on the $k_{660}(U_{10})$ parameterization obtained here.

4.2.2 Dual tracer method

For k_{660} measured using the DT method, we define an adaptation factor α_{DT} to estimate the impact of using a variable n, similar to Equation 17 for the EC method:

$$\alpha_{DT} = \frac{(660/Sc(^3He))^{-n(U_{10})}}{(660/Sc(^3He))^{-1/2}} \frac{1-(Sc(SF_6)/Sc(^3He))^{-1/2}}{1-(Sc(SF_6)/Sc(^3He))^{-n(U_{10})}}. \tag{18}$$

The additional factors compared to Equation 17 originate from the occurrence of n in the derivation of k at ambient Sc for the dual tracer method (Eq. 11). The impact of a variable $n(U_{10})$ on k_{660} is maximal in warm water for low wind speeds (Fig. 5), where k is up to 35 % lower than when using $n = 1/2$. A significant decrease in k_{660} is observed for both the BELAS and the Knorr11 fits in a wide range of (U_{10}, SST)-space. It can surpass 25 % for wind speeds below $4\,\mathrm{m\,s^{-1}}$ and water temperatures above 5 °C (Fig. 5a and b). For a wind speed of $7\,\mathrm{m\,s^{-1}}$, the decrease is still 10–15 % for most of the considered temperature range. Conducting a DT experiment under BELAS conditions could lead to a maximum decrease of 22 % and an average decrease of 10 % of k_{660} by applying α_{DT} based on the BELAS $n(U_{10})$ fit. Using Knorr11 data and the $n(U_{10})$ fit for Knorr11, the maximum decrease would be 29 %, with an average decrease of 11 %. At water temperatures of around 6 °C and

https://doi.org/10.5194/egusphere-2026-4525
Preprint. Discussion started: 22 September 2026

wind speeds ranging from 6 to 12.5 $\mathrm{m\,s^{-1}}$, as used in the derivation of the k_{660} parameterization in Nightingale et al. (2000), the decrease would be <1 % for 12.5 $\mathrm{m\,s^{-1}}$, but 15 % for 6 $\mathrm{m\,s^{-1}}$. For the DT method, we suggest applying a variable n (Table 1) in the normalization of k to a reference Sc for low to medium wind speeds, particularly at high water temperatures.

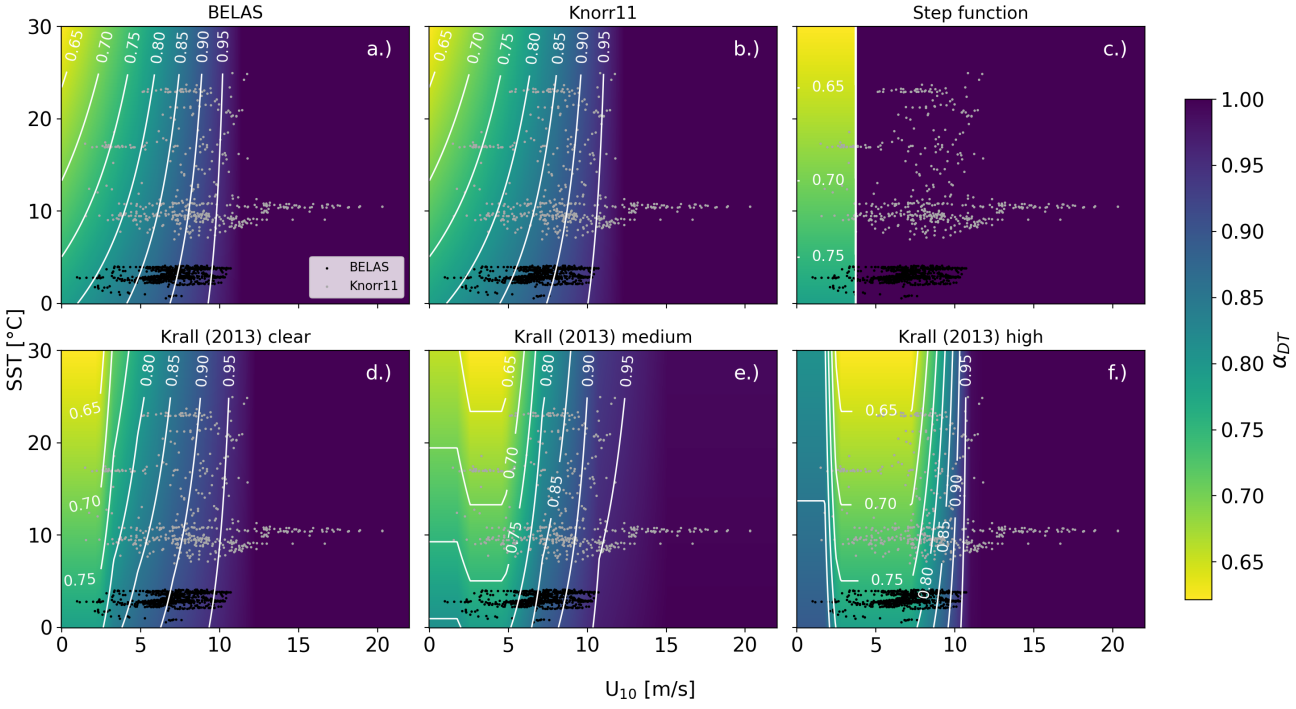

Figure 5. Relative change of DT gas transfer velocities when using a variable Schmidt number exponent compared to $n = 1/2$ for different $n(U_{10})$ relationships, based on a.) fitting BELAS CO_2 flux data, b.) fitting Knorr11 DMS gas transfer velocity data, c.) a stepfunction setting $n = 2/3$ for $U_{10} < 3.7\,\mathrm{m\,s^{-1}}$ and $n = 1/2$ for $U_{10} > 3.7,\mathrm{m\,s^{-1}}$, d.) laboratory results from Krall (2013) for surfactant-free conditions, e.) medium surfactant concentrations, and f.) high surfactant concentrations at the water surface. BELAS SST and U_{10} data is shown in black and Knorr11 SST and U_{10} data is shown in grey.

Similar to the EC-derived k_{660}, the maximum impact of using a variable n shifts towards slightly higher wind speeds for the DT method in the presence of surfactants under laboratory conditions (Krall, 2013). For the medium surfactant concentration case, the maximum is reached at 2.5–5 $\mathrm{m\,s^{-1}}$ (Fig. 5e), and at 2.5–7.5 $\mathrm{m\,s^{-1}}$ for the high surfactant concentration case (Fig. 5f). Implementing a step function for n with $n = 2/3$ for $U_{10} < 3.7\,\mathrm{m\,s^{-1}}$ and $n = 1/2$ for $U_{10} > 3.7\,\mathrm{m\,s^{-1}}$ would introduce a discontinuity in k of at least 20 % at the transition wind speed for the full range of water temperatures considered (Fig. 5c).

As for the EC method, under open-ocean conditions typically a constant $n = 1/2$ is applied for the DT method (Ho et al., 2006, 2011). In this case, for winds above 7 $\mathrm{m\,s^{-1}}$, there is agreement between k_{660} for CO_2 obtained from the DT method and k_{660} for CO_2 derived from the EC method, while estimates from the DT method are significantly lower at low wind speeds

https://doi.org/10.5194/egusphere-2026-4525
Preprint. Discussion started: 22 September 2026

(Yang et al., 2022). This discrepancy between EC and DT parameterizations of $k_{660}(U_{10})$ increases when a variable n is used, as k_{660} tends to increase for the EC method, whereas it decreases for the DT method.

4.2.3 Impact on global k_{660}

To estimate the impact of a variable n on global k_{660}, the adaptation factors α_{EC} and α_{DT} are determined based on monthly averages of hourly ERA5 reanalysis data for SST and U_{10} for 2023 (Hersbach et al., 2023), which is provided by the European Centre for Medium-Range Weather Forecasts (ECMWF). For the EC method, relative increases in k_{660} of more than 10 % occur in the Southern Ocean in January, and in the northern marginal seas of the North Atlantic and North Pacific in July (Fig. 6a and c). Calculating the area–weighted average of α_{EC} including all months results in a relative decrease of about 1 % on average. To estimate the relative change in global k_{660}, we use a global adaptation factor α_{EC}^{global} for 2023:

$$\alpha_{EC}^{\text{global}} = \frac{\sum\limits_{\text{months}} \alpha_{EC}\, k_{660}(U_{10})\, A_{\text{cell}}}{\sum\limits_{\text{months}} k_{660}(U_{10})\, A_{\text{cell}}}. \tag{19}$$

Here, $A_{\text{cell}} = A_{\text{cell}}(\text{lat}, \text{lon})$ denotes the grid cell area, and both α_{EC} and $k_{660}(U_{10})$ are given per grid cell and month. Only grid cells with a monthly ERA5 sea–ice cover of less than 15 % have been considered. Using the EC-derived $k_{660}(U_{10})$ parameterization of Yang et al. (2022), we obtain $|\alpha_{EC}^{global} - 1| < 0.2\,\%$, indicating that the effect on the EC-derived global k_{660} is negligible. The same holds true for the parameterization of Dong et al. (2021a), suggesting that the choice of parameterization has only a minor influence on this estimate. As the same Sc normalization factor with the Sc of CO_2 is used for both the EC method and the ^{14}C method (Eq. 7 and Eq. 12), the impact on the ^{14}C-derived global k_{660} is expected to be similar to that for the EC method.

Alternatively, the parameterizations shown in Fig. 4 based on BELAS data can be used in Equation 19. In this case, $k_{660}^{n=n(U_{10})} = 0.238U_{10}^2 + 3.646$ replaces $\alpha_{EC}\, k_{660}(U_{10})$ in the numerator, while $k_{660}(U_{10}) = 0.235U_{10}^2 + 2.948$ is used in the denominator. The global EC-derived k_{660} is then estimated to increase by around 5 %. This difference from the α_{EC}-based derivation is expected, as the parameterizations imply larger relative increases at low wind speeds than α_{EC}, as well as relative increases at wind speeds above $12\,\text{m}\,\text{s}^{-1}$ (Fig. 4). While α_{EC} describes the impact on an individual k_{660} value as a function of SST and U_{10}, the fitted parameterizations include the effects of bin averaging and the constraints imposed on the variability of $k_{660}(U_{10})$ by the chosen fit function. It is worth emphasizing that in the α_{EC}-based derivation, the same $k_{660}(U_{10})$ parameterization is used in both the numerator and the denominator of Equation 19, while the effect of a variable n is fully incorporated into α_{EC}.

For the DT method, relative decreases of at least 15 % are found across substantial regions of the global oceans, with maxima of 30 % or more in parts of the tropics and subtropics in both January and July (Fig. 6b and d). Taking the area–weighted average of α_{DT} across all months results in a relative decrease of around 16 % on average, with monthly values ranging from 15 % in July to 18 % in March. To estimate the impact on the DT-derived global k_{660}, we define a global adaptation factor α_{DT}^{global}

https://doi.org/10.5194/egusphere-2026-4525
Preprint. Discussion started: 22 September 2026

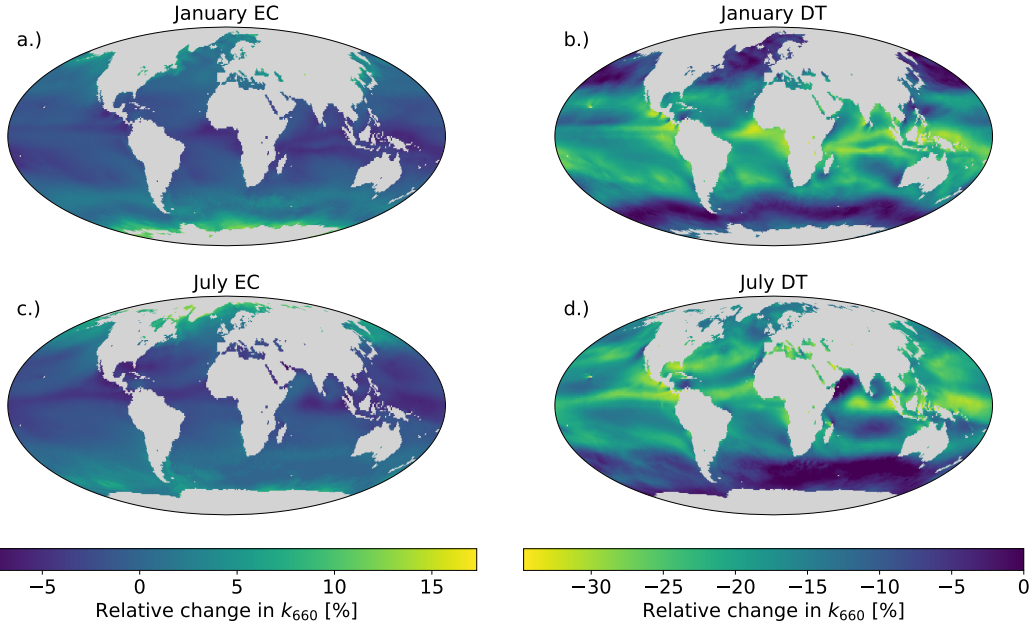

Figure 6. Relative change of k_{660} when using a variable Schmidt number exponent compared to $n = 1/2$. Adaptation factors α_{EC} and α_{DT} are calculated from ERA5 data on SST and U_{10}. Panels display a.) $\alpha_{EC} - 1$ for January 2023, b.) $\alpha_{DT} - 1$ for January 2023, c.) $\alpha_{EC} - 1$ for July 2023, and d.) $\alpha_{DT} - 1$ for July 2023. For a.)-d.), the fit parameters from BELAS data for $n = n(U_{10})$ are applied.

analogous to Equation 19:

$$\alpha_{DT}^{\text{global}} = \frac{\sum\limits_{\text{months}} \alpha_{DT}\, k_{660}(U_{10})\, A_{\text{cell}}}{\sum\limits_{\text{months}} k_{660}(U_{10})\, A_{\text{cell}}}. \tag{20}$$

Using the DT-derived $k_{660}(U_{10})$ parameterization of Nightingale et al. (2000) results in a decrease in k_{660} of around 12 %. A similar result is obtained using the parameterization of Ho et al. (2006), indicating that the choice of parameterization has only a minor influence on this estimate. Both parameterizations were renormalized from $Sc = 600$ to $Sc = 660$ before being inserted into Equation 20.

4.3 Impact on air–sea CO_2 flux calculations

4.3.1 Eddy covariance method

By applying the k_{660}-parameterizations derived in Sect. 4.2.1, an adaptation factor β_{EC} can be derived to estimate the impact of using a variable n on the derivation of air–sea gas fluxes via Equation 7. It is given by the ratio of the fitted $k_{660}(U_{10})$ parameterizations for BELAS (Fig. 4) and the inverse Sc normalization factors for $n(U_{10})$ and $n = 1/2$:

$$\beta_{EC} = \frac{(0.238\,U_{10}^2 + 3.646)(Sc/660)^{-n(U_{10})}}{(0.235\,U_{10}^2 + 2.948)(Sc/660)^{-1/2}}. \tag{21}$$

https://doi.org/10.5194/egusphere-2026-4525
Preprint. Discussion started: 22 September 2026

It is determined based on monthly averages of hourly ERA5 reanalysis data on SST and U_{10} (Hersbach et al., 2023). The parameterization component of β_{EC} leads to increasing fluxes, with large relative increases occurring at low wind speeds (Fig. 4). For the normalization component of β_{EC}, the fluxes increase for SST > 20 °C, where $Sc < 660$, with a greater impact at lower wind speeds. For SST < 20 °C, where $Sc > 660$, the fluxes decrease, with a greater impact at lower wind speeds. At SST values close to 20 °C, β_{EC} is primarily controlled by the parameterization component.

To estimate the global air–sea CO_2 fluxes in 2023, an average of global fCO_2-based flux data products was calculated (Friedlingstein et al., 2025; Hauck et al., 2025). Using the average as a proxy for fluxes derived based on EC parameterizations of $k_{660}(U_{10})$ enables us to estimate the impact of employing a variable n on air–sea CO_2 fluxes in different oceans. Scaling the fluxes with the adaptation factor β_{EC} leads to an estimation of the change in CO_2 flux (Fig. 7). In January, relative increases of 13 % or more are observed in large areas of the tropical and subtropical oceans, which coincide with areas of low wind speed and high water temperatures. Slight decreases of less than 3 % occur in cold waters, e.g. in the Southern Ocean near Antarctica. In July, areas with increases of 13 % or more shift north compared to January. The largest individual values are 29.6 % off the coast of Sulawesi in January and -4.1 % close to Antarctica in January. The observed impacts are generally of the same order of magnitude as the reported standard uncertainty in the EC-based k parameterizations of around 7 % at moderate wind speeds (Yang et al., 2022), although regional maxima can substantially exceed this level.

Applying β_{EC} to the average of the flux data products for January (Fig. 7a) results in an increase in outgassing of $0.12\,\mathrm{molC\,m^{-2}\,yr^{-1}}$ or more in the central Pacific. Assuming a total ocean uptake of CO_2 of around $3\,\mathrm{GtC\,yr^{-1}}$ for 2023 (Friedlingstein et al., 2025), $0.12\,\mathrm{molC\,m^{-2}\,yr^{-1}}$ roughly corresponds to 17 % of the average air–sea CO_2 flux. Large increases in outgassing are also observed in January in the South Atlantic, the South Pacific, and the Indian Ocean. Large increases in uptake of $0.13\,\mathrm{molC\,m^{-2}\,yr^{-1}}$ or more are primarily found in the North Atlantic and the North Pacific. In July 2023, increases in outgassing of more than $0.12\,\mathrm{molC\,m^{-2}\,yr^{-1}}$ are additionally observed in the Mediterranean Sea, around the Arabian Peninsula, in parts of the southern North Atlantic, and in parts of the southern North Pacific. Increases in uptake of $0.13\,\mathrm{molC\,m^{-2}\,yr^{-1}}$ or more are primarily found in the South Pacific and the southern Indian Ocean. The maximum increase in outgassing is observed in a patch close to the coast of Central America in January, reaching $0.50\,\mathrm{molC\,m^{-2}\,yr^{-1}}$. Uptake increases by up to $1.30\,\mathrm{molC\,m^{-2}\,yr^{-1}}$ in the Caspian Sea in July. The area–weighted average of the flux changes for all months yields a 6.6–9.5 % increase in outgassing, with the lowest increase observed in July and the highest in April. Uptake increases by 3.3–3.9 %, with the minimum in February and the maximum in August. An increase in net uptake is observed for most months, ranging from 0.8 % in July to 2.2 % in December. Decreases in net uptake are observed for August (-0.9 %) and September (-0.1 %). Global net uptake for 2023 is estimated to increase by 1.2 %.

As discussed in Sect. 4.2.1, using a variable Sc exponent for the EC method can significantly increase k_{660} for low wind speeds and cold water temperatures. These conditions are frequently met in the Southern Ocean and in the northern marginal seas of the North Atlantic and North Pacific, such as the Labrador Sea. Therefore, the k_{660} parameterization derived from BELAS data using a variable n shows a relative increase compared to $n = 1/2$, particularly at low wind speeds (Fig. 4). It is worth emphasizing again that applying the Sc normalization factors in Equation 21 amplifies this effect for SST > 20 °C and counteracts it for SST < 20 °C, with a greater impact at lower wind speeds. The effect of the normalization factors only

https://doi.org/10.5194/egusphere-2026-4525
Preprint. Discussion started: 22 September 2026

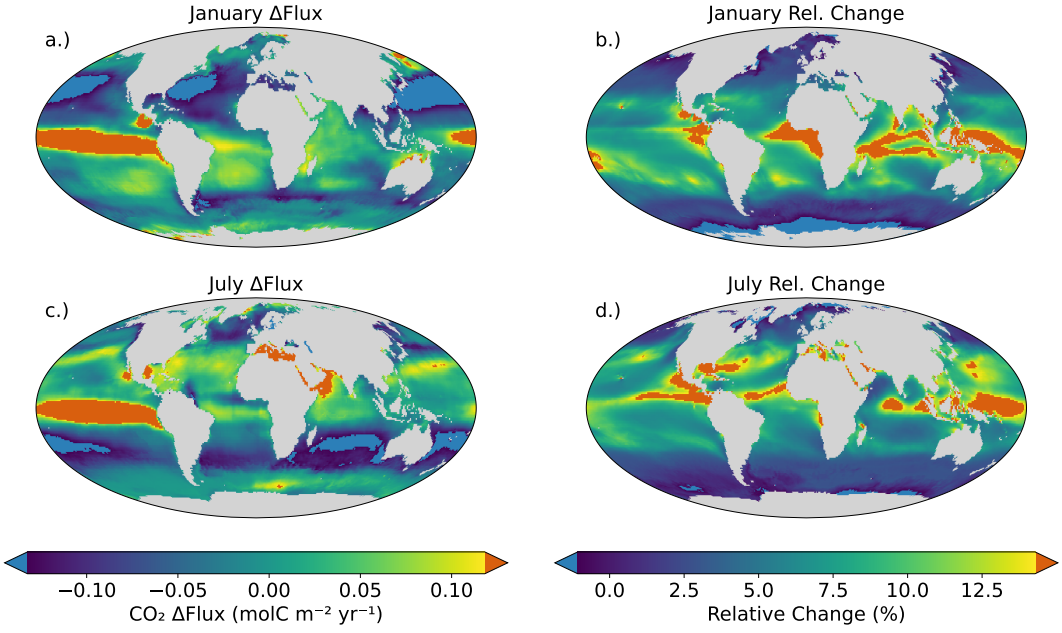

Figure 7. Change of air–sea CO_2 fluxes when using a variable Schmidt number exponent compared to $n = 1/2$. Results are based on flux data products derived from fCO_2 for 2023 (Friedlingstein et al., 2025). The flux change is estimated based on the average of all products for a.) January 2023 and c.) July 2023. Adaptation factors β_{EC} are calculated from ERA5 data on SST and U_{10}. The relative change in fluxes for January and July 2023 given by the adaptation factors is depicted in b.) and d.), respectively. For the changes in flux and the relative changes, the 5 percentile tails are not shown in the colorbars. The highest 5 percentile is colored in orange and the lowest 5 percentile is colored in blue. For a.)-d.), the fit parameters from BELAS data for $n = n(U_{10})$ are applied.

exceeds that of the parameterizations in cold waters, such as in the Southern Ocean, where values of $\beta_{EC} < 1$ can occur. The combined impact leads to a significant relative increase of air–sea gas fluxes in large areas of the global ocean (Figs. 3b and 3d). Coinciding with strong air–sea CO_2 fluxes, large increases in outgassing are observed e.g. in the central Pacific Ocean. Large increases in uptake occur in the southern North Atlantic and North Pacific in January and in the Southern Pacific and southern Indian Ocean in July. However, area–weighted averaging for all months suggests an increase in global net uptake of only 1.2 % in 2023 when using a variable n. Similarly, for the ^{14}C k_{660}-based flux estimates, the impact on the global ocean is not expected to be significant.

4.3.2 Dual tracer method

The flux data products that were used to investigate the impact of a variable n for EC parameterizations can also be treated as if they were based on DT-derived k using Equation 7. The impact of the k_{660} parameterization used and the Sc normalization factor is analogous to that discussed for the EC method, except there is a decrease in k for all wind speeds. However, it is not possible to investigate this in detail here, as was done for the EC method in Fig. 4, because there is no DT dataset of k available

https://doi.org/10.5194/egusphere-2026-4525
Preprint. Discussion started: 22 September 2026

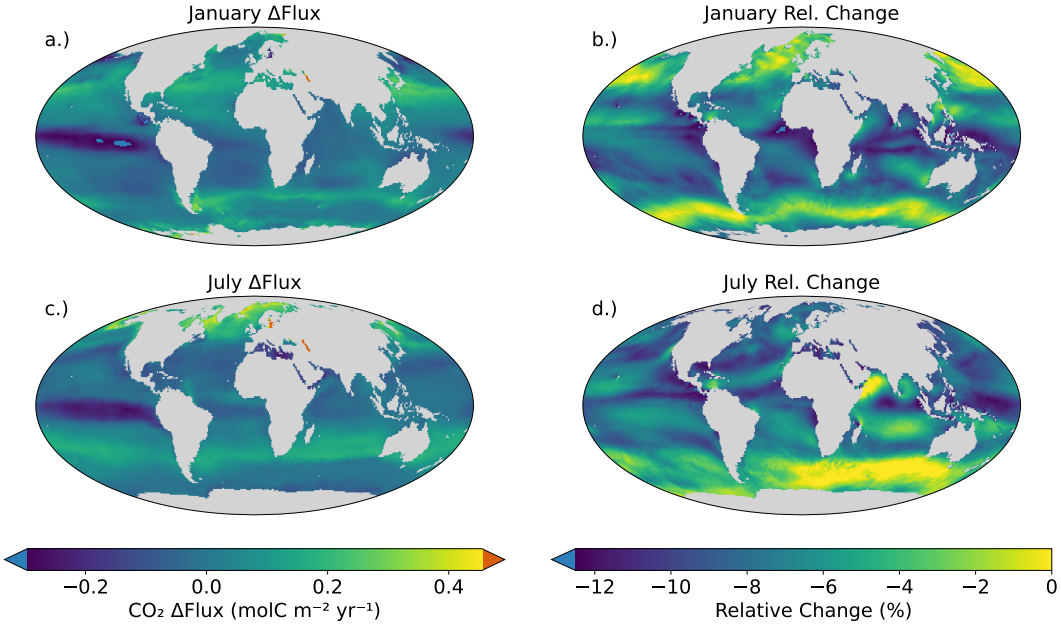

Figure 8. Same as Fig. 7, but deriving the adaptation factors β_{DT} for the DT method via Equation 22. These factors exclusively consider the direct dependence of k on n, and do not take into account the impact of using a variable n on the fitting of a DT-derived $k_{660}(U_{10})$ parameterization. For the changes in flux, the 0.1 percentile tails are not included in the colorbar. The highest 0.1 percentile is colored in orange and the lowest 0.1 percentile is colored in blue. For the relative changes, only the minimum 0.1 percentile is excluded from the colorbar.

for this analysis. But the DT-derived k at ambient Sc, as given by Equation 11, has an additional direct dependence on n. The impact of this dependence on CO_2 fluxes using DT-derived parameterizations can be accessed without assuming a particular parameterization by scaling with an adaptation factor β_{DT}:

$$\beta_{DT} = \frac{1 - \left(Sc(SF_6)/Sc(^3He)\right)^{-1/2}}{1 - \left(Sc(SF_6)/Sc(^3He)\right)^{-n(U_{10})}}. \tag{22}$$

Relative decreases in fluxes of around 10 % or greater are observed in certain regions of the tropics for January and July, as well as in some areas of the South Atlantic and South Pacific in January, and in some areas of the North Atlantic and North Pacific in July (Fig. 8). Decreases of around 5 % are found in substantial regions of the global oceans, extending from 45°S to 35°N in January and north of 35°S in July. The highest 0.1 percentile of relative decreases is primarily found in coastal waters within the tropics and subtropics, with the highest individual value of -13.5 % being reached off the coast of Sulawesi. In January, further significant decreases are observed in a patch in the tropical Atlantic Ocean.

The application of β_{DT} to the average flux data products results in a decrease in uptake of 0.2 $\mathrm{molC\,m^{-2}\,yr^{-1}}$ or more in two bands at around 35°S and 40 °N in January (Fig. 8a). Meanwhile, a decrease in outgassing of around 0.2 $\mathrm{molC\,m^{-2}\,yr^{-1}}$ is observed in the central Pacific Ocean. In July, the two bands shift northwards to around 30°S and 60°N. Additionally, a decrease

https://doi.org/10.5194/egusphere-2026-4525
Preprint. Discussion started: 22 September 2026

in outgassing of around 0.2 $\mathrm{molC\,m^{-2}\,yr^{-1}}$ is observed in the Mediterranean Sea. Values below -0.3 $\mathrm{molC\,m^{-2}\,yr^{-1}}$ occur in January in the central Pacific Ocean and in two patches close to the coast of Central America. Values above 0.45 $\mathrm{molC\,m^{-2}\,yr^{-1}}$ are observed in the Caspian Sea and in gaps in the Arctic and Antarctic sea ice in January, reaching 0.83 $\mathrm{molC\,m^{-2}\,yr^{-1}}$ in the Caspian Sea. The greatest decreases of uptake in July occur in the Baltic Sea, north of Iceland, and in the Caspian Sea, with values reaching 1.12 $\mathrm{molC\,m^{-2}\,yr^{-1}}$. Calculating the area–weighted average of the flux changes for all months yields a 5.6–7.9 % decrease in outgassing, with the lowest decrease observed in July and the highest in March. Uptake decreases by 4.6–6.1 %, with the minimum in December and the maximum in June. A decrease in net uptake is observed for all months, ranging from 3.5 % in January to 5.9 % in June. Global net uptake for 2023 is estimated to decrease by 4.6 %.

Based on the direct dependence of the DT-derived k on n, using a variable Sc exponent for the DT method can significantly impact the resulting fluxes by 5 % to 12 % or more for low to medium wind speeds. Relatively low winds coincide with large air–sea CO_2 fluxes in the tropical Pacific Ocean in 2023, as well as in two circumpolar bands: one in the mid- to high latitudes of the Northern Hemisphere, and one in the mid-latitudes of the Southern Hemisphere. Area–weighted averaging for all months indicates a global net uptake decrease of around 5 % for 2023. The observed impact of the direct dependence of k on n is of the same order of magnitude as the reported standard uncertainty in the DT-based k parameterizations of 5–10 % (Woolf et al., 2019). Additionally, the Sc normalization chosen for parameterizing the DT gas transfer velocity affects the resulting air–sea CO_2 flux in a manner similar to that observed for the EC method, but it leads to a further decrease in k.

5 Conclusions

Since the 1980s, theoretical considerations have indicated that the Sc exponent n can vary from $n = 2/3$ for a smooth surface to $n = 1/2$ for a wavy surface (Jähne, 1980; Liss and Merlivat, 1986; Jähne et al., 1987). However, a variable n has not been widely adopted, as the impact on the air–sea gas transfer velocity k was generally assumed to be negligible, the exact shape of the transition is unknown, and it is difficult to measure n in the field. Instead, a constant Sc exponent of $n = 1/2$ was commonly implemented when normalizing k for both the EC and DT methods in oceans. For lakes, a step function with $n = 2/3$ for low wind speeds and $n = 1/2$ for medium to high wind speeds was frequently applied. Here, we derived parameterizations $n(U_{10})$ using TKE dissipation rate ϵ and EC air–sea gas flux data for CO_2 and DMS from the Labrador Sea and the North Atlantic. Based on data collected during the BELAS experiment, we obtained $n(U_{10}) = -(0.0136 \pm 0.0026)\,U_{10} + 2/3$. For poorly soluble gases beyond CO_2 and DMS, whose air–sea exchange is primarily waterside controlled, the parameterizations of n presented here are also expected to be applicable. For highly soluble gases such as methanol, the parameterizations of n can still be applied to the waterside transfer velocity, but the effect on the total k is expected to be negligible because air–sea exchange is primarily airside controlled. To further constrain $n(U_{10})$, simultaneous EC flux measurements of two poorly soluble gases could be conducted to access n more directly via the ratio of the measured k.

We investigated the effect of using a variable n on k and the air–sea CO_2 flux for both the EC and the DT method. Implementing a step function for n introduces a discontinuity in k_{660} at the transition wind speed. If a step function has to be applied, our results suggest that a reasonable choice for the transition wind speed would be 6–8 $\mathrm{m\,s^{-1}}$ instead of 3–4 $\mathrm{m\,s^{-1}}$.

https://doi.org/10.5194/egusphere-2026-4525
Preprint. Discussion started: 22 September 2026

For the EC method, the relative increase of k_{660} can exceed 10 % at wind speeds below around 6 ms^{-1} and water temperatures below 10 °C. These conditions are frequently met in parts of the Southern Ocean and the marginal seas of the North Atlantic and North Pacific during local summer. Global k_{660} for 2023 is estimated to increase by 5 % or less. Applying a k_{660} parameterization with variable n, while using EC data collected during the BELAS experiment for the fit of k_{660}, can impact the resulting air–sea CO_2 fluxes by more than 13 %. In areas with large air–sea CO_2 fluxes, this can result in an increase of the estimated outgassing or increase of the estimated uptake by 0.1 $\mathrm{molC\,m^{-2}yr^{-1}}$ or more. However, global net uptake for 2023 is estimated to increase by only about 1 %. For the EC method under low winds and low water temperatures, we suggest applying a variable exponent when normalizing the gas transfer velocity to a reference Schmidt number.

For the DT method, the impact on k_{660} can reach a 15–35 % decrease for low to medium wind speeds, with particularly large values observed for high water temperatures. These conditions are frequently met in tropical and subtropical oceans, as well as seasonally in mid-latitude oceans. Global k_{660} for 2023 is estimated to decrease by around 12 %. The application of the Sc normalization factor with a variable n and a parameterization of k_{660} to derive CO_2 fluxes is analogous to the EC method, but leads to a decrease in fluxes. Additionally, the DT gas transfer velocity is directly dependent on n. Without using specific parameterizations, it can be estimated that this dependence has an impact on the CO_2 flux of 5–12 % at low to medium wind speeds, with larger effects at lower wind speeds. This coincides with large air–sea CO_2 fluxes in the tropical Pacific Ocean and in two circumpolar bands in 2023. Absolute changes in flux reach 0.2 $\mathrm{molC\,m^{-2}\,yr^{-1}}$ in these regions. Global net uptake for 2023 is estimated to decrease by about 5 % when using a variable n. For the DT method under low to medium winds, we suggest applying a variable Sc exponent, particularly at high water temperatures.

Data availability. This study used ERA5 reanalysis data (Hersbach et al., 2023) downloaded from https://doi.org/10.24381/cds.adbb2d47. Further data used in this study are available by requesting the corresponding author.

Author contributions. SFH, LE, and BW conceptualized the study, and YD contributed to the development of the analysis methodology. SFH performed the data analysis and prepared the figures, supervised by LE and BW. BW served as chief scientist for the BELAS field campaign, in which SFH and KM participated. KM, BW, and ATD processed the ASIP data, and BW curated the dataset. SFH processed the EC data. SFH wrote the original draft of the manuscript. All authors commented on the paper and helped improve it.

Competing interests. The authors declare no conflicts of interest relevant to this study.

Acknowledgements. SFH thanks the University of Bonn for the internal funding for his PhD position. LE acknowledges support from Formas, the Swedish Research Council for Sustainable Development (2020-02305_3), and the Bonn Global Collaboration Fund of the University of Bonn, which allowed SFH to visit the AirSea Lab in Galway. BW was supported by the Irish Centre for Research in Applied Geosciences

https://doi.org/10.5194/egusphere-2026-4525
Preprint. Discussion started: 22 September 2026

(iCRAG) under Grant No. 13/RC/2092_2, funded by Research Ireland. We extend our thanks to the captain and crew of the RV Knorr and the RV Celtic Explorer for making this study possible.

https://doi.org/10.5194/egusphere-2026-4525
Preprint. Discussion started: 22 September 2026

References

Bade, D.: Gas Exchange at the Air–Water Interface, pp. 70–78, Elsevier, https://doi.org/10.1016/B978-012370626-3.00213-1, 2009.

Bell, T., Landwehr, S., Miller, S., de Bruyn, W., Callaghan, A., Scanlon, B., Ward, B., Yang, M., and Saltzman, E. S.: Estimation of bubble-mediated air–sea gas exchange from concurrent DMS and CO_2 transfer velocities at intermediate–high wind speeds, Atmospheric Chemistry and Physics, 17, 9019–9033, https://doi.org/10.5194/acp-17-9019-2017, 2017.

Bell, T. G.: Quantifying the effect of bubbles upon air-sea gas exchange, presentation at SOLAS Open Science Conference 2015, 2015.

Blomquist, B., Brumer, S., Fairall, C., Huebert, B., Zappa, C., Brooks, I., Yang, M., Bariteau, L., Prytherch, J., Hare, J., Czerski, H., Matei, A., and Pascal, R.: Wind Speed and Sea State Dependencies of Air-Sea Gas Transfer: Results From the High Wind Speed Gas Exchange Study (HiWinGS), J. Geophys. Res. Oceans, 122, 8034–8062, https://doi.org/10.1002/2017JC013181, 2017.

Bodmer, P., Barbosa, P., Bilodeau, F., Nadeau, D. F., Parkes, A. H., Rust, F., Thiboult, A., Tremblay, A., and del Giorgio, P. A.: Spatial Dependence of Gas Transfer Velocity in Boreal Reservoirs, Journal of Geophysical Research: Biogeosciences, 130, e2025JG008 994, https://doi.org/10.1029/2025JG008994, https://agupubs.onlinelibrary.wiley.com/doi/abs/10.1029/2025JG008994, 2025.

Brumer, S., C.J. Zappa, C., Blomquist, B., Fairall, C., Cifuentes-Lorenzen, A., Edson, J., Brooks, I., and Huebert, B.: Wave-Related Reynolds Number Parameterizations of CO2 and DMS Transfer Velocities, Geophys. Res. Lett., 44, 9865–9875, https://doi.org/10.1002/2017GL074979, 2017.

Butterworth, B. and Miller, S.: Air-sea exchange of carbon dioxide in the Southern Ocean and Antarctic marginal ice zone, Geophys. Res. Lett., 43, 7223–7230, https://doi.org/10.1002/2016GL069581, 2016.

Coantic, M.: A model of gas transfer across air-water interfaces with capillary waves, J. Geophys. Res. Oceans, 91, 3925–3943, https://doi.org/10.1029/JC091iC03p03925, 1986.

Deacon, E. L.: Gas transfer to and across an air–water interface, Tellus, 29, 363–374, 1977.

Di Giorgio, S., Pirozzoli, S., and Iafrati, A.: Air Entrainment and Gas Transfer in Wave Breaking Events, Geophys. Res. Lett., 52, e2025GL114 907, https://doi.org/10.1029/2025GL114907, 2025.

Dobashi, R. and Ho, D.: Air–sea gas exchange in a seagrass ecosystem – results from a ^3He / SF_6 tracer release experiment, Biogeosciences, 20, 1075–1087, https://doi.org/10.5194/bg-20-1075-2023, 2023.

Dong, Y., Yang, M., Bakker, D., Liss, P., Kitidis, V., Brown, I., Chierici, M., Fransson, A., and Bell, T.: Near-Surface Stratification Due to Ice Melt Biases Arctic Air-Sea CO2 Flux Estimates, Geophys. Res. Lett., 48, e2021GL095 266, https://doi.org/10.1029/2021GL095266, 2021a.

Dong, Y., Yang, M., Bakker, D. C. E., Kitidis, V., and Bell, T. G.: Uncertainties in eddy covariance air–sea CO2 flux measurements and implications for gas transfer velocity parameterisations, Atmos. Chem. Phys., 21, 8089–8110, https://doi.org/10.5194/acp-21-8089-2021, 2021b.

Dong, Y., Bakker, D. C. E., Bell, T. G., Yang, M., Landschützer, P., Hauck, J., Rödenbeck, C., Kitidis, V., Bushinsky, S. M., and Liss, P. S.: Direct observational evidence of strong CO_2 uptake in the Southern Ocean, Science Advances, 10, eadn5781, https://doi.org/10.1126/sciadv.adn5781, 2024.

Dong, Y., Jähne, B., Woolf, D., Krall, K., Yang, M., Czerski, H., Liang, J.-H., Brooks, I., McNeil, C., Wanninkhof, R., Ho, D., Atamanchuk, D., and Marandino, C.: The Role of Bubbles in Air-Sea Gas Exchange: A Critical Review, ESS Open Archive, https://doi.org/10.22541/essoar.175611263.31332921/v1, 2025a.

https://doi.org/10.5194/egusphere-2026-4525
Preprint. Discussion started: 22 September 2026

Dong, Y., Yang, M., Bell, T. G., Marandino, C., and Woolf, D.: Asymmetric bubble-mediated gas transfer enhances global ocean CO_2 uptake, Nature Communications, 10595, https://doi.org/10.1038/s41467-025-66652-5, 2025b.

Dong, Y., Marandino, C., Dobashi, R., Ho, D., Rehder, G., Bittig, H., Karnatz, J., Sabbaghzadeh, B., Czerski, H., and Engel, A.: Mechanisms of air–sea CO_2 exchange in the central Baltic Sea, Atmos. Chem. Phys., 26, 5567–5587, https://doi.org/10.5194/acp-26-5567-2026, https://acp.copernicus.org/articles/26/5567/2026/, 2026.

Erkkilä, K.-M., Ojala, A., Bastviken, D., Biermann, T., Heiskanen, J., Lindroth, A., Peltola, O., Rantakari, M., Vesala, T., and Mammarella, I.: Methane and carbon dioxide fluxes over a lake: comparison between eddy covariance, floating chambers and boundary layer method, Biogeosciences, 15, 429–445, https://doi.org/10.5194/bg-15-429-2018, 2018.

Esters, L., Landwehr, S., Sutherland, G., Bell, T. G., Christensen, K. H., Saltzman, E. S., Miller, S. D., and Ward, B.: Parameterizing air-sea gas transfer velocity with dissipation, J. Geophys. Res. Oceans, 122, 3041–3056, https://doi.org/10.1002/2016JC012088, 2017.

Esters, L., Rutgersson, A., Nilsson, E., and E.Sahlée: Non-local Impacts on Eddy-Covariance Air–Lake CO_2 Fluxes., Bound.-Lay. Meteorol., 178, 283–300, https://doi.org/10.1007/s10546-020-00565-2, 2021.

Ford, D., Blannin, J., Watts, J., Watson, A., Landschützer, P., Jersild, A., and Shutler, J.: A Comprehensive Analysis of Air-Sea CO2 Flux Uncertainties Constructed From Surface Ocean Data Products, Glob. Biogeochem. Cycles, 38, e2024GB008 188, https://doi.org/10.1029/2024GB008188, https://agupubs.onlinelibrary.wiley.com/doi/abs/10.1029/2024GB008188, 2024.

Friedlingstein, P., O'Sullivan, M., Jones, M. W., Andrew, R. M., Hauck, J., Landschützer, P., Quéré, C. L., Li, H., Luijkx, I. T., Olsen, A., Peters, G. P., Peters, W., Pongratz, J., Schwingshackl, C., Sitch, S., Canadell, J. G., Ciais, P., Jackson, R. B., Alin, S. R., Arneth, A., Arora, V., Bates, N. R., Becker, M., Bellouin, N., Berghoff, C. F., Bittig, H. C., Bopp, L., Cadule, P., Campbell, K., Chamberlain, M. A., Chandra, N., Chevallier, F., Chini, L. P., Colligan, T., Decayeux, J., Djeutchouang, L. M., Dou, X., Rojas, C. D., Enyo, K., Evans, W., Fay, A. R., Feely, R. A., Ford, D. J., Foster, A., Gasser, T., Gehlen, M., Gkritzalis, T., Grassi, G., Gregor, L., Gruber, N., Gürses, O., Harris, I., Hefner, M., Heinke, J., Hurtt, G. C., Iida, Y., Ilyina, T., Jacobson, A. R., Jain, A. K., Jarníková, T., Jersild, A., Jiang, F., Jin, Z., Kato, E., Keeling, R. F., Goldewijk, K. K., Knauer, J., Korsbakken, J. I., Lan, X., Lauvset, S. K., Lefèvre, N., Liu, Z., Liu, J., Ma, L., Maksyutov, S., Marland, G., Mayot, N., McGuire, P. C., Metzl, N., Monacci, N. M., Morgan, E. J., Nakaoka, S.-I., Neill, C., Niwa, Y., Nützel, T., Olivier, L., Ono, T., Palmer, P. I., Pierrot, D., Qin, Z., Resplandy, L., Roobaert, A., Rosan, T. M., Rödenbeck, C., Schwinger, J., Smallman, T. L., Smith, S. M., Sospedra-Alfonso, R., Steinhoff, T., Sun, Q., Sutton, A. J., Séférian, R., Takao, S., Tatebe, H., Tian, H., Tilbrook, B., Torres, O., Tourigny, E., Tsujino, H., Tubiello, F., van der Werf, G., Wanninkhof, R., Wang, X., Yang, D., Yang, X., Yu, Z., Yuan, W., Yue, X., Zaehle, S., Zeng, N., and Zeng, J.: Global Carbon Budget 2024, Earth System Science Data, 17, 965–1039, https://doi.org/10.5194/essd-17-965-2025, https://essd.copernicus.org/articles/17/965/2025/, 2025.

Gloege, L. and Eisaman, M.: Regional Uncertainty Analysis in the Air–Sea CO2 Flux, Earth and Space Science, 12, e2024EA004 032, https://doi.org/10.1029/2024EA004032, 2025.

Golub, M., Koupaei-Abyazani, N., Vesala, T., Mammarella, I., Ojala, A., Bohrer, G., Weyhenmeyer, G., Blanken, P., Eugster, W., Koebsch, F., et al.: Diel, seasonal, and inter-annual variation in carbon dioxide effluxes from lakes and reservoirs, Environmental Research Letters, 18, https://doi.org/10.1088/1748-9326/acb834, 2023.

Guérin, F., Abril, G., Serça, D., Delon, C., Richard, S., Delmas, R., Tremblay, A., and Varfalvy, L.: Gas transfer velocities of CO2 and CH4 in a tropical reservoir and its river downstream, Journal of Marine Systems, 66, 161–172, https://doi.org/10.1016/j.jmarsys.2006.03.019, 2007.

Gutiérrez-Loza, L., Nilsson, E., Wallin, M. B., Sahlée, E., and Rutgersson, A.: On physical mechanisms enhancing air–sea CO_2 exchange, Biogeosciences, 19, 5645–5665, https://doi.org/10.5194/bg-19-5645-2022, 2022.

https://doi.org/10.5194/egusphere-2026-4525
Preprint. Discussion started: 22 September 2026

Gålfalk, M., Bastviken, D., Fredriksson, S., and Arneborg, L.: Determination of the piston velocity for water-air interfaces using flux chambers, acoustic Doppler velocimetry, and IR imaging of the water surface, J. Geophys. Res. Biogeosci., 118, 770–782, https://doi.org/10.1002/jgrg.20064, 2013.

Hauck, J., Mayot, N., Landschützer, P., and Jersild, A.: Global Carbon Budget 2024, surface ocean fugacity of CO2 (fCO2) and air-sea CO2 flux of individual global ocean biogeochemical models and surface ocean fCO2-based data-products, https://doi.org/10.5281/zenodo.14639761, https://doi.org/10.5281/zenodo.14639761, 2025.

Hersbach, H., Bell, B., Berrisford, P., Biavati, G., Horányi, A., Sabater, J. M., Nicolas, J., Peubey, C., Radu, R., Rozum, I., Schepers, D., Simmons, A., Soci, C., Dee, D., and Thépaut, J.-N.: ERA5 hourly data on single levels from 1940 to present [Dataset]. Copernicus Climate Change Service (C3S) Climate Data Store (CDS), https://doi.org/10.24381/cds.adbb2d47., 2023.

Ho, D. and Wanninkhof, R.: Air–sea gas exchange in the North Atlantic: 3He/SF6 experiment during GasEx-98, Tellus B: Chem. and Phys. Meteor., 68, 30 198, https://doi.org/10.3402/tellusb.v68.30198, 2016.

Ho, D., Wanninkhof, R., Schlosser, P., Ullman, D., Hebert, D., and Sullivan, K.: Toward a universal relationship between wind speed and gas exchange: Gas transfer velocities measured with 3He/SF6 during the Southern Ocean Gas Exchange Experiment, J. Geophys. Res. Oceans, 116, https://doi.org/10.1029/2010JC006854, 2011.

Ho, D. T., Law, C. S., Smith, M. J., Schlosser, P., Harville, M., and Hill, P.: Measurements of air-sea gas exchange at high wind speeds in the Southern Ocean: Implications for global parameterizations, Geophys. Res. Lett., 33, 16 611 – 16 616, https://doi.org/10.1029/2006GL026817, 2006.

Jähne, B.: Air-sea gas exchange, in: Encyclopedia Ocean Sciences, edited by Steele, J. H., Turekian, K. K., and Thorpe, S. A., pp. 3434–3444, Elsevier, 2009.

Jähne, B. and Haußecker, H.: Air–water gas exchange, Annu. Rev. Fluid Mech., 30, 443–468, https://doi.org/10.1146/annurev.fluid.30.1.443, 1998.

Jähne, B.: Zur Parametrisierung des Gasaustauschs mit Hilfe von Laborexperimenten, Ph.D. thesis, Institut für Umweltphysik, Fakultät für Physik und Astronomie, Univ. Heidelberg, 1980.

Jähne, B., Münnich, K., Bösinger, R., Dutzi, A., Huber, W., Werner, and Libner, P.: On the parameters influencing air-water gas exchange, J. Geophys. Res. Oceans, 92, 1937–1949, https://doi.org/10.1029/JC092iC02p01937, 1987.

Katul, G. and Liu, H.: Multiple mechanisms generate a universal scaling with dissipation for the air-water gas transfer velocity, Geophys. Res. Lett., 44, 1–7, https://doi.org/10.1002/2016GL072256, 2017.

Krall, K. E.: Laboratory Investigations of Air-Sea Gas Transfer under a Wide Range of Water Surface Conditions, PhD. Ruperto-Carola University of Heidelberg, Germany, 2013.

Lamont, J. C. and Scott, D. S.: An eddy cell model of mass transfer into the surface of a turbulent liquid, AlChE J., 16, 513–519, 1970.

Landwehr, S.: Ship Borne Direct Eddy Covariance Flux Measurements, Ph.D. thesis, NUI Galway, 2015.

Landwehr, S., O'Sullivan, N., and Ward, B.: Direct Flux Measurements from Mobile Platforms at Sea: Motion and Airflow Distortion Corrections Revisited, J. Atmos. Oceanic Technol., 32, 1163–1178, https://doi.org/10.1175/JTECH-D-14-00137.1, 2015.

Landwehr, S., Miller, S. D., Smith, M. J., Bell, T. G., Saltzman, E. S., and Ward, B.: Using eddy covariance to measure the dependence of air–sea CO_2 exchange rate on friction velocity, Atmos. Chem. Phys., 18, 4297–4315, https://doi.org/10.5194/acp-18-4297-2018, 2018.

Li, L., Bullee, P., Ellingsen, S., and Hearst, R.: Sub-surface turbulence or non-breaking capillary waves: which dominates air–water gas transfer?, J. Fluid Mech., 1009, A48, https://doi.org/10.1017/jfm.2025.242, 2025.

https://doi.org/10.5194/egusphere-2026-4525
Preprint. Discussion started: 22 September 2026

Liss, P. S. and Merlivat, L.: The Role of Air–Sea Exchange in Geochemical Cycling, chap. Air-Sea Gas Exchange Rates: Introduction and Synthesis, pp. 113–127, ed. P. Buat-Menard, Dordrecht, Holland: Kluwer Academic Publishers, 1986.

Lueck, R., Fer, I., Bluteau, C., Dengler, M., Holtermann, P., Inoue, R., LeBoyer, A., Nicholson, S.-A., Schulz, K., and Stevens, C.: Best practices recommendations for estimating dissipation rates from shear probes, Frontiers Mar. Sci., Volume 11 - 2024, https://doi.org/10.3389/fmars.2024.1334327, https://www.frontiersin.org/journals/marine-science/articles/10.3389/fmars.2024.1334327, 2024.

Mammarella, I., Nordbo, A., Rannik, U., Haapanala, S., Levula, J., Laakso, H., Ojala, A., Peltola, O., Heiskanen, J., Pumpanen, J., and Vesala, T.: Carbon dioxide and energy fluxes over a small boreal lake in Southern Finland, J. Geophys. Res. Biogeosci., 120, 1296–1314, https://doi.org/10.1002/2014JG002873, 2015.

McKenna, S. P. and McGillis, W. R.: The role of free–surface turbulence and surfactants in air–water gas transfer, Int. J. Heat Mass Trans., 47, 539–553, https://doi.org/10.1016/j.ijheatmasstransfer.2003.06.001, 2004.

Mears, C., Lee, T., Ricciardulli, L., Wang, X., and Wentz, F.: RSS Cross-Calibrated Multi-Platform (CCMP) 6-hourly ocean vector wind analysis on 0.25 deg grid, Version 3.0, Remote Sensing Systems, Santa Rosa, CA. https://doi.org/10.56236/RSS-uv6h30, 2022.

Miller, S. D., Marandino, C., and Saltzman, E. S.: Ship-based measurement of air-sea CO_2 exchange by eddy covariance, J. Geophys. Res., 115, https://doi.org/10.1029/2009JD012193, 2010.

Naegler, T.: Reconciliation of excess 14C-constrained global CO2 piston velocity estimates, Tellus B: Chemical and Physical Meteorology, 61, 372–384, https://doi.org/10.1111/j.1600-0889.2008.00408.x, 2009.

Nagel, L., Krall, K., and Jähne, B.: Measurements of air–sea gas transfer velocities in the Baltic Sea, Ocean Sci., 15, 235–247, https://doi.org/10.5194/os-15-235-2019, 2019.

Nightingale, P. D., Malin, G., Law, C. S., Watson, A. J., Liss, P. S., Liddicoat, M. I., Boutin, J., and Upstill-Goddard, R. C.: In situ evaluation of air-sea gas exchange parameterizations using novel conservative and volatile tracers, Glob. Biogeochem. Cycles, 14, https://doi.org/10.1029/1999GB900091, 2000.

Obertegger, U., Corradini, S., Cerasino, L., and Weiss, L.: Decadal changes in surface CO2 concentrations and CO2 fluxes in a mountain lake, Limnol. Oceanogr., 69, 1143–1156, https://doi.org/10.1002/lno.12557, 2024.

Paranaíba, J., Barros, N., Mendonça, R., Linkhorst, A., Isidorova, A., Roland, F., Almeida, R., and Sobek, S.: Spatially Resolved Measurements of CO2 and CH4 Concentration and Gas-Exchange Velocity Highly Influence Carbon-Emission Estimates of Reservoirs, Environmental Science & Technology, 52, 607–615, https://doi.org/10.1021/acs.est.7b05138, pMID: 29257874, 2018.

Prytherch, J. and Yelland, M.: Wind, Convection and Fetch Dependence of Gas Transfer Velocity in an Arctic Sea-Ice Lead Determined From Eddy Covariance CO2 Flux Measurements, Glob. Biogeochem. Cycles, 35, e2020GB006 633, https://doi.org/10.1029/2020GB006633, e2020GB006633 2020GB006633, 2021.

Reichardt, H.: Vollständige Darstellung der turbulenten Geschwindigkeitsverteilung in glatten Leitungen, ZAMM - J. Appl. Math. Mech., 7, 208–219, https://doi.org/10.1002/zamm.19510310704, 1951.

Richter, K. and Jähne, B.: A laboratory study of the Schmidt number dependency of air-water gas transfer, in: Gas Transfer at Water Surfaces 2010, edited by Komori, S., McGillis, W., and Kurose, R., pp. 322–332, Kyoto University Press, Kyoto, https://doi.org/10.5281/zenodo.14955, 2011.

Sweeney, C., Gloor, E., Jacobson, A. R., Key, R. M., McKinley, G., Sarmiento, J. L., and Wanninkhof, R.: Constraining global air-sea gas exchange for CO_2 with recent bomb ^{14}C measurements, Glob. Biogeochem. Cycles, 21, https://doi.org/10.1029/2006GB002784, 2007.

https://doi.org/10.5194/egusphere-2026-4525
Preprint. Discussion started: 22 September 2026

Wang, B., Liao, Q., Fillingham, J. H., and Bootsma, H. A.: On the coefficients of small eddy and surface divergence models for the air–water gas transfer velocity, J. Geophys. Res. Oceans, 120, 2129–2146, https://doi.org/10.1002/2014JC010253, 2015.

Wanninkhof, R.: Relationship between wind speed and gas exchange over the ocean, J. Geophys. Res., 97, 7373–7382, https://doi.org/10.1029/92JC00188, 1992.

Wanninkhof, R.: Relationship between wind speed and gas exchange over the ocean revisited, Limnol. and Oceanogr.: Methods, 12, 351–362, https://doi.org/10.4319/lom.2014.12.351, 2014.

Wanninkhof, R., Asher, W., Weppernig, R., Chen, H., Schlosser, P., Langdon, C., and Sambrotto, R.: Gas transfer experiment on Georges Bank using two volatile deliberate tracers, J. Geophys. Res. Oceans, 98, 20 237–20 248, https://doi.org/10.1029/93JC01844, 1993.

Wanninkhof, R., Sullivan, K., and Top, Z.: Air-sea gas transfer in the Southern Ocean, J. Geophys. Res. Oceans, 109, https://doi.org/10.1029/2003JC001767, 2004.

Wanninkhof, R., Asher, W. E., Ho, D. T., Sweeney, C., and McGillis, W. R.: Advances in quantifying air–sea gas exchange and environmental forcing, Ann. Rev. Mar. Sci., 1, 213–244, https://doi.org/10.1146/annurev.marine.010908.163742, 2009.

Ward, B., Fristedt, T., Callaghan, A. H., Sutherland, G., Sanchez, X., Vialard, J., and ten Doeschate, A.: The Air-Sea Interaction Profiler (ASIP): An Autonomous Upwardly Rising Profiler for Microstructure Measurements in the Upper Ocean, J. Atmos. Oceanic Technol., 31, 2246–2267, https://doi.org/10.1175/JTECH-D-14-00010.1, 2014.

Watson, A., Upstill-Goddard, R., and Liss, P.: Air–sea gas exchange in rough and stormy seas measured by a dual-tracer technique, Nature, 349, 145–147, https://doi.org/10.1038/349145a0, 1991.

Woolf, D. K., Shutler, J. D., Goddijn-Murphy, L., Watson, A. J., Chapron, B., Nightingale, P. D., Donlon, C. J., Piskozub, J., Yelland, M. J., Ashton, I., Holding, T., Schuster, U., Girard-Ardhuin, F., Grouazel, A., Piolle, J.-F., Warren, M., Wrobel-Niedzwiecka, I., Land, P. E., Torres, R., Prytherch, J., Moat, B., Hanafin, J., Ardhuin, F., and Paul, F.: Key Uncertainties in the Recent Air-Sea Flux of CO2, Glob. Biogeochem. Cycles, 33, 1548–1563, https://doi.org/10.1029/2018GB006041, https://agupubs.onlinelibrary.wiley.com/doi/abs/10.1029/2018GB006041, 2019.

Yang, M., Bell, T. G., Hopkins, F. E., Kitidis, V., Cazenave, P. W., Nightingale, P. D., Yelland, M. J., Pascal, R. W., Prytherch, J., Brooks, I. M., and Smyth, T. J.: Air–sea fluxes of CO_2 and CH_4 from the Penlee Point Atmospheric Observatory on the south-west coast of the UK, Atmospheric Chemistry and Physics, 16, 5745–5761, https://doi.org/10.5194/acp-16-5745-2016, 2016.

Yang, M., Bell, T., Bidlot, J.-R., Blomquist, B., Butterworth, B., Dong, Y., Fairall, C., Landwehr, S., Marandino, C., Miller, S., Saltzman, E., and Zavarsky, A.: Global Synthesis of Air-Sea CO2 Transfer Velocity Estimates From Ship-Based Eddy Covariance Measurements, Frontiers in Marine Science, Volume 9, https://doi.org/10.3389/fmars.2022.826421, 2022.

Zhao, D., Jia, N., and Dong, Y.: Relationship between turbulent energy dissipation and gas transfer through the air-sea interface, Tellus B: Chem. and Phys. Meteor., 70, 1–11, https://doi.org/10.1080/16000889.2018.1528133, 2018.